Acta Cryst. (1999). A**55**, 1026–1033

Anisotropic dispersion of the band structure and formation of ring patterns in CBED

L.-M. Peng[a,b]* and J. M. Zuo[c]

[a]*Department of Electronics, Peking University, Beijing 100871, People's Republic of China,* [b]*Beijing Laboratory of Electron Microscopy, Center for Condensed Matter Physics and Institute of Physics, Chinese Academy of Sciences, PO Box 2724, Beijing 100080, People's Republic of China, and* [c]*Department of Physics and Astronomy, Arizona State University, Tempe, AZ 85287-1504, USA. E-mail: lmpeng@lmplab.blem.ac.cn*

(*Received 14 April 1999; accepted 15 June 1999*)

Abstract

An off-axis ring pattern was observed in the $\langle 1\bar{1}1\rangle$ zone-axis CBED pattern of an NiO single crystal. The pattern was interpreted as resulting from anisotropic dispersion of the band structure of the two most strongly excited free Bloch waves and strong absorption of the most tightly bound 1*s* Bloch state. Comparison has also been made with the case of MgO which has the same structure as NiO but weaker scattering power. The tightly bound 1*s* Bloch state in MgO was found to play an important role together with a strongly excited free Bloch state and a more conventional zone-axis ring pattern similar to that observed in the $\langle 001\rangle$ zone-axis CBED pattern of silicon was observed.

1. Introduction

In this paper, we discuss an off-axis ring pattern observed in the $\langle 1\bar{1}1\rangle$ zone-axis convergent-beam electron diffraction (CBED) patterns from a single crystal of NiO. Previously, various types of zone-axis patterns were investigated by Steeds and colleagues for simple crystals with f.c.c. and b.c.c. structures (Shannon & Steeds, 1977), and transition-metal dichalcogenides (Fung & Steeds, 1984). In this paper, we investigate zone-axis CBED patterns of compounds with the sodium chloride structure, in particular the ring patterns, and interpret the formation of the ring patterns using a two-Bloch-wave approximation (Hirsch *et al.*, 1977).

Within the framework of the Bloch-wave method, the diffracted beam intensities may be expressed as

$$I_g(\mathbf{K}_t) = \left| \sum_j \alpha^{(j)}(\mathbf{K}_t) C_g^{(j)}(\mathbf{K}_t) \exp\{2\pi i \gamma^{(j)}(\mathbf{K}_t) t\} \right|^2, \quad (1)$$

in which $\mathbf{K}_t$ is the tangential component of the incident electron wavevector $\mathbf{k}_0$ parallel to the entrance surface of the crystal, t is the thickness of the crystal, $\alpha^{(j)}$ is the excitation amplitude of the jth Bloch wave, $\gamma^{(j)}$ and $C_g^{(j)}$ are the eigenvalues and eigenvectors of the following Schrödinger equation (Bethe, 1928):

$$[K^2 - (\mathbf{k}_0 + \gamma^{(j)}\mathbf{n} + \mathbf{g})^2] C_g^{(j)} + \sum_g U_{g-h} C_h^{(j)} = 0, \quad (2)$$

where $\mathbf{n}$ is a unit vector along the surface normal, $K^2 = 2mE/\hbar^2$, with E being the energy of the primary electron beam, and U_g is the gth Fourier coefficient of the scaled crystal potential $U(\mathbf{r}) = 2mV(\mathbf{r})/\hbar^2$. In general, the diffracted-beam intensity I_g is a complicated function of the incident-beam direction, *i.e.* $I_g = I_g(\mathbf{K}_t)$, and the contrast results from the many interference terms between different Bloch waves.

An extremely important conclusion resulting from the early investigations on Bloch waves by Hirsch *et al.* (1977), Steeds *et al.* (Shannon & Steeds, 1977) and more recently by Gjønnes *et al.* (1988, 1989) is that, although for near-zone-axis incidence many diffracted beams are excited and the diffraction situation is always a many-beam case, only a few Bloch waves are appropriately excited and in many situations the number of effective Bloch waves is as few as two or three. For the case of two Bloch waves, the expression for the diffracted-beam intensities becomes

$$I_g(\mathbf{K}_t) = |\alpha^{(1)} C_g^{(1)}|^2 + |\alpha^{(2)} C_g^{(2)}|^2 + 2\Re\{\alpha^{*(1)}\alpha^{(2)} C_g^{*(1)} C_g^{(2)}\} \times \cos\{2\pi(\gamma^{(2)} - \gamma^{(1)})t\}, \quad (3)$$

i.e. a fringe pattern is expected for a two-Bloch-wave case. In this article, we show that basic features of the off-axis ring pattern observed in the NiO $\langle 1\bar{1}1\rangle$ zone-axis pattern may be explained based on this simple two-Bloch-wave approximation.

2. Basics of NiO and crystals with the sodium chloride structure

NiO belongs to a very important class of materials, *i.e.* transition-metal oxides. What makes this class of materials interesting is the correlation effects resulting from the strong Coulomb interaction between electrons and the many unusual properties exhibited by these materials resulting from the complicated interplay between the Coulomb interaction and the influence of the magnetic ordering. A single crystal of NiO is antiferromagnetic at room temperature and paramagnetic above its Néel temperature T_N of 523 K. At temperatures above T_N, the crystal structure of NiO is sodium

chloride, consisting of an equal number of cations, such as Ni^{2+} and Mg^{2+}, and anions, such as O^{2-}, sitting at alternate points of a simple cubic lattice, *i.e.* the cation and anion form an interpenetrating f.c.c. lattice. Below T_N, the crystal becomes slightly distorted from its cubic structure to a rhombohedral one (Slack, 1960). The distortion consists of contraction of the high-temperature cubic unit cell along one of the cubic ⟨111⟩ directions, and the amount of distortion increases with decreasing temperature. In this paper, all experiments and simulations have been made at temperatures below T_N and we therefore use the rhombohedral notation. For the convenience of comparison with cubic lattice notation, we note here that the $\langle 1\bar{1}1\rangle$ axis of the rhombohedral lattice corresponds to the ⟨001⟩ axis of the cubic lattice, and 110 and 011 reflections of the rhombohedral lattice correspond to 200 and 020 of the cubic lattice, respectively.

3. Results and discussion

All CBED patterns were obtained using a liquid-nitrogen cold stage, an LEO 912 Ω electron microscope and imaging plates. The temperature at the specimen was estimated to be 106 K, and the primary-beam energy was calibrated to be 119.52 keV using higher-order Laue-zone (HOLZ) line patterns. Shown in Fig. 1(*a*) is an experimental $\langle 1\bar{1}1\rangle$ zone-axis CBED pattern obtained from an NiO sample. The pattern consists of the central transmitted (000) disc, four {110} and four {121} discs.

Near the center of the transmitted (000) disc, an elliptical pattern composed of fine lines is clearly visible. These fine lines result from interactions involving HOLZ reflections, and the pattern is a manifestation of the rhombohedral lattice distortion, for if the lattice was cubic the envelope of the HOLZ lines in the central region would have been a circle instead of an ellipse, see Eaglesham *et al.* (1988). The object of this paper is, however, not the pattern of fine HOLZ lines. Instead, we are interested in the broad ring pattern composed of rings centered around the four corners of the central (000) disc pointing along the {121} directions. Shown in Fig. 1(*b*) is a simulated zone-axis CBED pattern corresponding to the experimental conditions of Fig. 1(*a*) and a crystal thickness of $t = 2750$ Å using 193 beams. The Debye–Waller factors used in the simulation are $B_{\mathrm{Ni}} = 0.1349$ and $B_{\mathrm{O}} = 0.2384$ Å^{-2}, which correspond to a specimen temperature of 106.15 K (Gao *et al.*, 1999). Although all features including the fine HOLZ lines and the off-axis ring pattern have been well reproduced in the simulated pattern, the many-beam simulation does not provide much insight into the origin of the formation of the off-axis ring pattern. In what follows, we shall discuss the basic features of this pattern *via* analysis of the behavior of the most strongly excited Bloch waves and their corresponding band structures.

Bloch waves are waves that are compatible with the translation symmetry of crystals. Different Bloch waves may have different forms and be excited differently by the incident high-energy electrons. A Bloch wave is characterized fully by two quantities, *i.e.* its eigenvalue $\gamma^{(j)}$ and corresponding eigenvector $C_g^{(j)}$; both are functions of $\mathbf{K}_t$. The surface composed of $\gamma^{(j)}(\mathbf{K}_t)$ is usually referred to as the *dispersion surface* (Hirsch *et al.*, 1977).

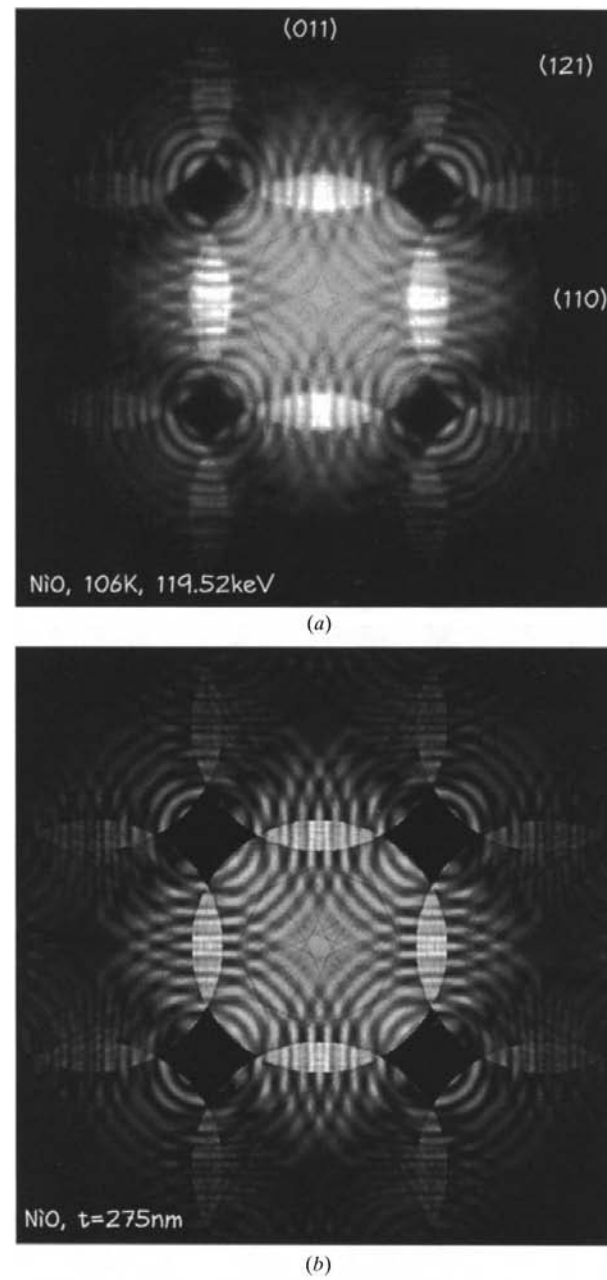

Fig. 1. (*a*) Experimental and (*b*) simulated $\langle 1\bar{1}1\rangle$ zone-axis CBED patterns obtained from an NiO crystal. The pattern was recorded at 106 K for a primary-beam energy of 119.15 keV, and the simulation was made for a crystal thickness of t = 2750 Å using 193 beams.

A useful alternative is the *band structure* (Bird, 1989), which is related to the dispersion surface *via* the following relation:

$$S^{(j)}(\mathbf{K}_t) = 2K\{K - k_{0_z} - \gamma^{(j)}(\mathbf{K}_t)\}, \tag{4}$$

where k_{0_z} is the component of the incident electron wavevector $\mathbf{k}_0$ along the z axis. The usefulness of the band-structure picture is that it gives a direct indication as to whether the corresponding Bloch wave is bound or free, *i.e.* for $S^{(j)} < 0$ the Bloch state is a bound state localizing around one of the atomic strings, for $S^{(j)} > 0$, the Bloch state is a free state that is more delocalized in space and may travel in the crystal over a long distance without being absorbed.

The number of possible Bloch waves existing in a crystal may be infinite, but which of these Bloch waves will contribute to the total wave field in a crystal depends on the boundary conditions. The excitations of these Bloch waves are described by the *excitation amplitude* $\alpha^{(j)}(\mathbf{K}_t)$. Shown in Fig. 2 are plots of the band structure $S^{(j)}(\mathbf{K}_t)$ and corresponding excitation strength $|\alpha^{(j)}(\mathbf{K}_t)|$ of the first five most strongly excited Bloch waves for $\mathbf{K}_t$ lying along the ⟨110⟩ direction. These plots indicate that of all the possible Bloch waves one bound Bloch state with $S^{(1)} < 0$ and two free Bloch states with $S^{(2)} > 0$ and $S^{(3)} > 0$ dominate. Similar plots (shown in Fig. 3) along the ⟨121⟩ direction show that the picture is basically the same, except that towards the edge an additional Bloch wave begins to become appropriately excited. Basically, the wave field is determined by three Bloch waves, *i.e.* the number 1 bound Bloch state and two free Bloch waves, number 2 and number 3.

The first impression of the ring pattern shown in Fig. 1 is that it is in fact a simple fringe pattern, suggesting that the pattern is formed by interference between two Bloch waves rather than three as suggested by Figs. 2 and 3. Trial simulations using the three most strongly excited Bloch waves reveal that, of the three Bloch waves, only the two free Bloch waves contribute significantly to the

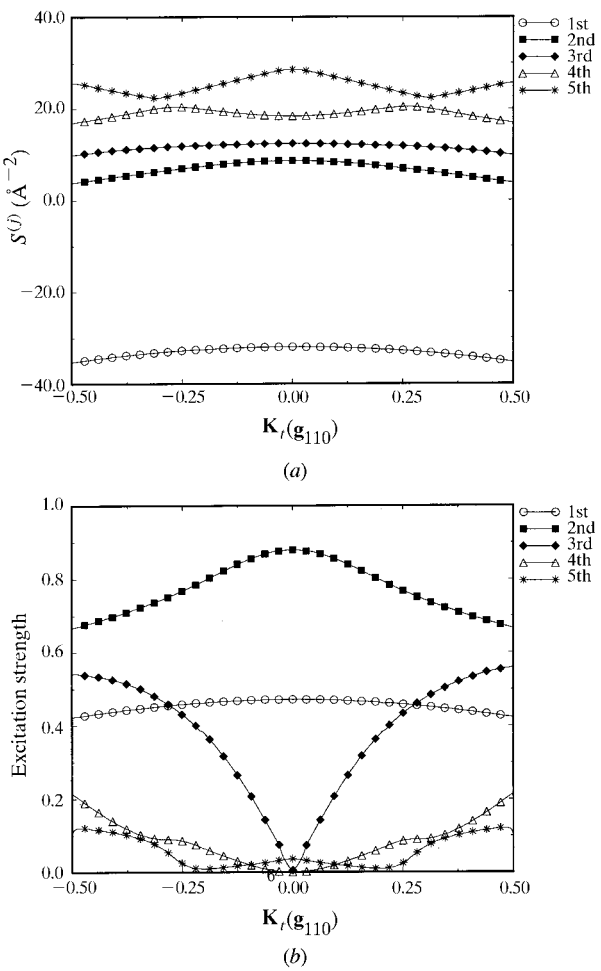

Fig. 2. Plots of (*a*) band structure, *i.e.* $S^{(j)}(\mathbf{K}_t)$, and (*b*) corresponding excitation strengths, $|\alpha^{(j)}(\mathbf{K}_t)|$, of the first five most strongly excited Bloch waves along the ⟨110⟩ direction.

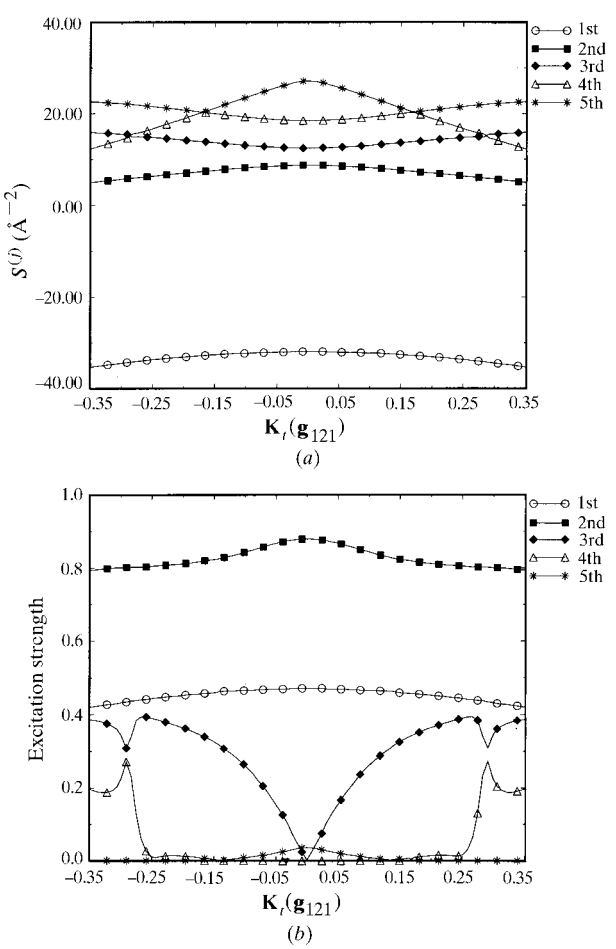

Fig. 3. Plots of (*a*) band structure, *i.e.* $S^{(j)}(\mathbf{K}_t)$, and (*b*) corresponding excitation strengths, $|\alpha^{(j)}(\mathbf{K}_t)|$, of the first five most strongly excited Bloch waves along the ⟨121⟩ direction.

contrast observed in the CBED pattern of NiO as shown in Fig. 1(*a*), and these are Bloch waves numbers 2 and 3. Shown in Fig. 4(*a*) is a simulated CBED pattern using only Bloch waves numbers 2 and 3. The basic features of the off-axis ring pattern observed experimentally have already been reproduced here. With an additional free Bloch wave, *i.e.* Bloch wave number 4, the resulting CBED pattern is seen to be almost identical to that simulated using all Bloch waves (Fig. 4*d*), and the inclusion of the bound Bloch wave number 1 in Fig. 4(*c*) does not have noticeable effect compared to Fig. 4(*b*) using only free Bloch waves. Shown in Fig. 4(*e*) is the difference map $\delta S(\mathbf{K}_t) = S^{(3)}(\mathbf{K}_t) - S^{(2)}(\mathbf{K}_t)$, and in Fig. 4(*f*) is the surface $S^{(1)}(\mathbf{K}_t)$ for the tightly bound Bloch wave number 1. These results suggest that the basic features of the off-axis ring pattern may be analyzed by using the two-Bloch-wave approximation to write the intensity of the transmitted beam as

$$I_0(\mathbf{K}_t) = |C_0^{(2)}(\mathbf{K}_t)|^4 + |C_0^{(3)}(\mathbf{K}_t)|^4 + 2|C_0^{(2)}(\mathbf{K}_t)|^2|C_0^{(3)}(\mathbf{K}_t)|^2 \times \cos\{2\pi[\gamma^{(3)}(\mathbf{K}_t) - \gamma^{(2)}(\mathbf{K}_t)]t\}. \quad (5)$$

Roughly speaking, the CBED pattern changes between $I_0(\text{max.})(\mathbf{K}_t)$ (Fig. 5*b*),

$$I_0(\text{max.}) = |C_0^{(2)}(\mathbf{K}_t)|^4 + |C_0^{(3)}(\mathbf{K}_t)|^4 + 2|C_0^{(2)}(\mathbf{K}_t)|^2|C_0^{(3)}(\mathbf{K}_t)|^2,$$

and $I_0(\text{min.})$ (Fig. 5*c*),

$$I_0(\text{min.}) = |C_0^{(2)}(\mathbf{K}_t)|^4 + |C_0^{(3)}(\mathbf{K}_t)|^4 - 2|C_0^{(2)}(\mathbf{K}_t)|^2|C_0^{(3)}(\mathbf{K}_t)|^2,$$

and the off-axis ring pattern results mainly from the strong anisotropic dispersion of the difference surface $\delta S(\mathbf{K}_t)$ between $S^{(3)}(\mathbf{K}_t)$ and $S^{(2)}(\mathbf{K}_t)$, as shown in Fig. 4(*e*). The term anisotropic dispersion means that the difference surface $\delta S(\mathbf{K}_t)$ depends not only on the magnitude of $\mathbf{K}_t$ but also on its direction, *e.g.* the plots of $S^{(j)}(\mathbf{K}_t)$ are different for $\mathbf{K}_t$ lying along ⟨110⟩ and ⟨121⟩ directions as shown in Figs. 2 and 3. As a comparison, we show in Fig. 4(*f*) the dispersion surface of the tightly bound Bloch state number 1. It is seen that to a good approximation this surface is isotropic, *i.e.* the dispersion is independent of the direction of $\mathbf{K}_t$. This is because electrons trapped in this tightly bound state are highly localized to the atom string composed of Ni and O atoms along the $\langle 1\bar{1}1\rangle$ zone axis and are hardly affected by the presence of neighboring atom strings. In other words, this tightly bound state, a 1*s*-type state, is essentially determined by an atom string with cylindrical symmetry as if the neighboring atom strings were absent. The dispersion surface of this tightly bound state is therefore isotropic or of cylindrical symmetry. The free Bloch waves, on the other hand, are affected strongly by the two-dimensional spatial arrangement of atom strings. The dispersion surfaces of these free Bloch waves depend, therefore, on the arrangement of the atom strings and are in general anisotropic.

The fringes appearing in Fig. 1 may be regarded as extinction distance contours and the formation of the contours may be described with the help of Fig. 5(*a*), which is the map of extinction distances resulting from interference between Bloch waves numbers 2 and 3, *i.e.* $\zeta^{(3-2)}(\mathbf{K}_t) = 1/2[\gamma^{(3)}(\mathbf{K}_t) - \gamma^{(2)}(\mathbf{K}_t)]$. For small crystal thickness satisfying $t \ll \zeta^{(3-2)}(\mathbf{K}_t)$, the cosine function on the right-hand side of equation (5) deviates little

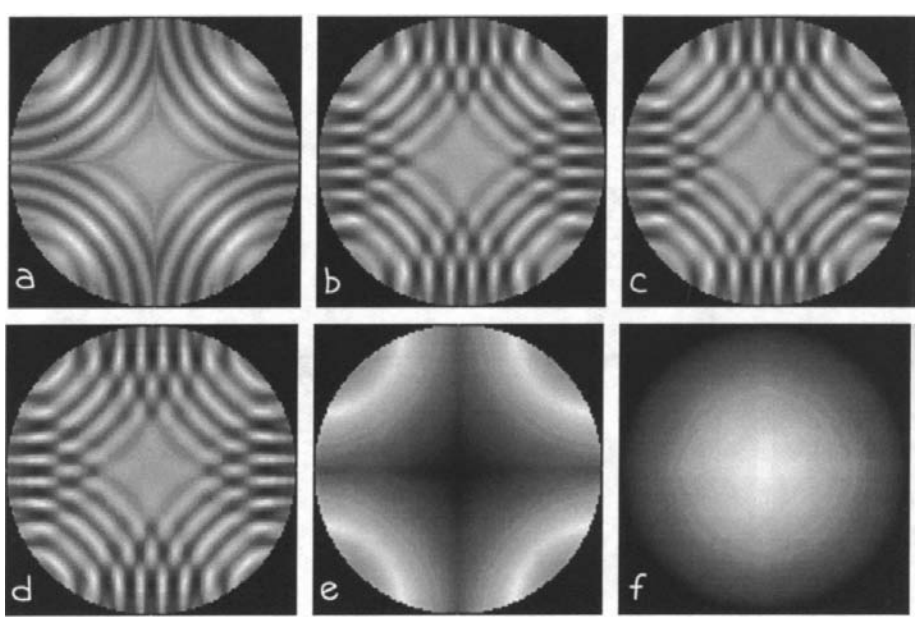

Fig. 4. CBED patterns of the transmitted disc formed by (*a*) two Bloch waves, numbers 2 and 3; (*b*) three Bloch waves, numbers 2, 3 and 4; (*c*) four Bloch waves, numbers 1, 2, 3 and 4; (*d*) all Bloch waves. Shown in (*e*) is the map of $S^{(3)}(\mathbf{K}_t) - S^{(2)}(\mathbf{K}_t)$ and in (*f*) is the map of $S^{(1)}(\mathbf{K}_t)$.

from unity for all points in the CBED disc. We have therefore $I_0(\mathbf{K}_t) \approx I_0(\text{max.})$. This is seen to be the case for a crystal thickness of 50 Å as shown in Fig. 5(*d*) [which is rather similar to the I_0(max.) map as shown in Fig. 5(*b*)]. As the crystal thickness increases, the phase factor on the right-hand side of equation (5), $2\pi[\gamma^{(3)} - \gamma^{(2)}]t$, first approaches π around the four corners of Fig. 5(*a*) at a thickness of 189 Å, or in other words the crystal thickness t first approaches the extinction distance $\zeta^{(3-2)}(\mathbf{K}_t)$ around the four corners, and the pattern therefore becomes dark firstly around the four corners (see Fig. 5*e*), which is rather similar to I_0(min.) as shown in Fig. 5(*c*). As the crystal thickness increases further, more fringes appear as shown in Figs. 5(*g*)–(*i*). This is because for a thicker crystal less change in $\delta\gamma$ will give a phase change of π. For a fixed range of $\delta\gamma_{\max} - \delta\gamma_{\min}$, more fringes will therefore be produced. For all patterns, it is seen that the contrast near the center of the disc does not change. This is because Bloch wave number 3 is hardly excited near the center of the disc, *i.e.* near the zone axis, and the transmitted and diffracted beam intensities are then determined entirely by Bloch wave number 2 and are therefore thickness independent.

We now consider Bloch wave number 1. Figs. 2 and 3 amply demonstrate that Bloch wave number 1 is strongly excited for all points in the transmitted CBED disc. This Bloch wave does not, however, contribute much to the observed contrast of the CBED patterns. The reason is related to the fact that this Bloch wave is indeed a tightly bound state with negative value of $S^{(1)}$. In a real-space representation (Fig. 6*a*), it is seen that this bound state is highly localized around the atom strings. It is expected therefore that this Bloch wave will be strongly absorbed, *i.e.* attenuated. Quantitatively, this is manifested by a large value of the imaginary part of the eigenvalue, *i.e.* $\Im\{\gamma^{(1)}\} = \mu^{(1)}$. The intensity of the Bloch wave is then given by

$$I^{(1)}(\mathbf{r}) = \left|\alpha^{(1)} \sum_g C_g^{(1)} \exp\{2\pi i \mathbf{g}\cdot\mathbf{r}\} \exp(2\pi i \gamma^{(1)} t)\right|^2$$
$$= I^{(1)}(x, y, z = 0) \exp(-4\pi\mu t).$$

For the tightly bound Bloch wave number 1, the length of absorption $\ell = 1/(4\pi\mu) = 400$ Å. A crystal of thickness $t = \ell$ will then lose 63% of electrons from the elastic wave field, suggesting that the tightly bound Bloch wave will hardly contribute to the CBED pattern contrast at larger thicknesses such as 2750 Å as used in simulating Fig. 1(*b*). For a zone-axis incidence, the lengths of absorption ℓ for other significant free Bloch waves are all more than 10 000 Å. These free Bloch

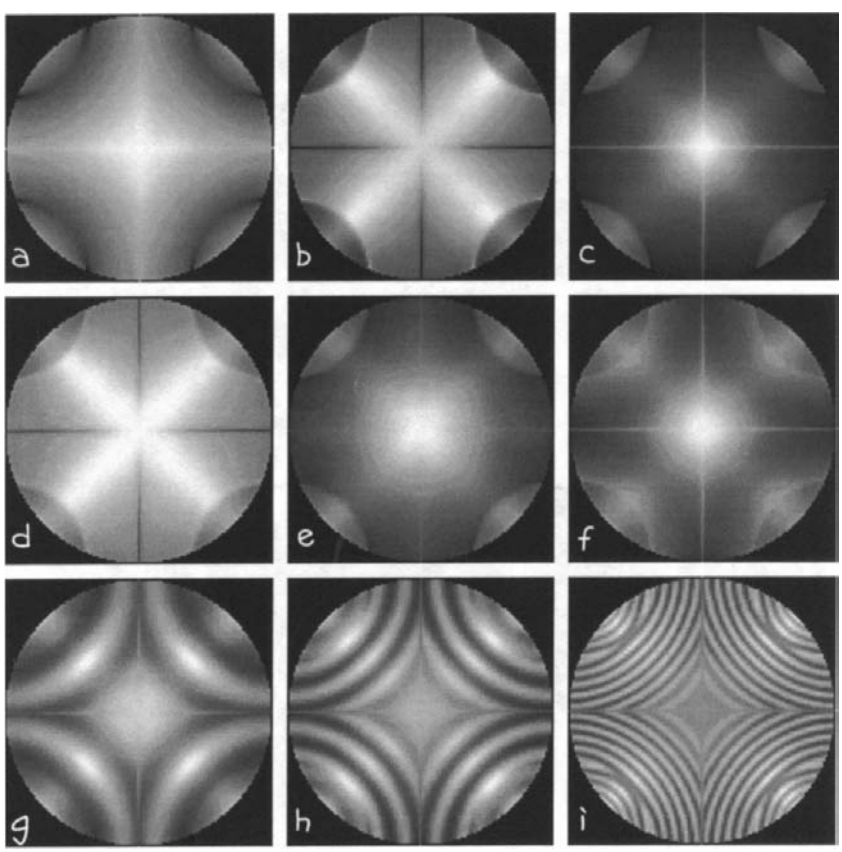

Fig. 5. CBED patterns of the transmitted (000) disc formed by two Bloch waves, numbers 2 and 3, and for thicknesses (*d*) t = 50 Å; (*e*) t = 189 Å; (*f*) t = 300 Å; (*g*) t = 1000 Å; (*h*) t = 2000 Å and (*i*) t = 5000 Å. Shown in (*a*) is the difference map $\delta\gamma^{(4,2)}(\mathbf{K}_t) = \gamma^{(4)}(\mathbf{K}_t) - \gamma^{(2)}(\mathbf{K}_t)$; and in (*b*) is the maximum and in (*c*) is the minimum $I_0(\mathbf{K}_t)$ map (see text for details).

waves are sometimes also called *channelling Bloch waves* to indicate that they may channel through a crystal without being absorbed rapidly.

Among the metal oxides with the sodium chloride structure, NiO is relatively strong in scattering power. An interesting question is how the ring pattern changes as the scattering power decreases, and in what follows we shall consider the case of MgO. Shown in Fig. 7 is a simulated zone-axis CBED pattern corresponding to the same diffraction conditions as Fig. 1(*b*) and with the same crystal thickness. This figure shows clearly that for MgO the ring pattern is dominated by a different type of zone-axis ring pattern, which is similar to that observed in the ⟨001⟩ zone-axis pattern of silicon, see for example Tanaka & Terauchi (1985).

To investigate the origin for the formation of the different ring pattern shown in Fig. 7, we calculated the band structure $S^{(j)}(\mathbf{K}_t)$ for MgO and results for the first five most strongly excited Bloch states are shown in Fig. 8 for a line profile along the ⟨110⟩ direction. The plot of excitation strength $|\alpha^{(j)}(\mathbf{K}_t)|$ shows clearly that the wave field is dominated by Bloch waves numbers 1 and 2, of which the Bloch wave number 1 is a 1*s*-type bound state with negative value of $S^{(1)}(\mathbf{K}_t)$, and Bloch wave number 2 is a free Bloch state with positive value of $S^{(2)}(\mathbf{K}_t)$.

Shown in Fig. 9(*a*) is a simulated CBED pattern for the transmitted (000) disc corresponding to the central part of Fig. 7. Shown in Figs. 9(*b*) and 9(*c*) are, respectively, the $S^{(1)}(\mathbf{K}_t)$ and $S^{(2)}(\mathbf{K}_t) - S^{(1)}(\mathbf{K}_t)$ maps. While for the first bound Bloch states the $S^{(1)}(\mathbf{K}_t)$ surface is basically isotropic, the $S^{(2)}(\mathbf{K}_t) - S^{(1)}(\mathbf{K}_t)$ surface shown in Fig. 9(*c*) is anisotropic with four flat edges towards the {110} directions and a similar broad shape to the CBED ring pattern shown in Fig. 9(*a*). Fig. 9(*d*) shows the CBED pattern formed by Bloch waves numbers 1 and 2, and Fig. 9(*e*) shows that formed by Bloch waves numbers 1, 2 and 3. It is seen that the zone-axis ring pattern has already been reproduced well by the first two Bloch waves. While Bloch wave number 3 introduces some modulation to the zone-axis ring pattern, the basic features of the pattern remain the same and are determined mainly by the interference between Bloch waves numbers 1 and 2. Shown in Fig. 9(*f*) is the extinction distance map $\zeta^{(1-2)}(\mathbf{K}_t) = 1/2(\gamma^{(2)} - \gamma^{(1)})$ between Bloch waves numbers 1 and 2. The dark regions towards the four edges indicate that the corresponding

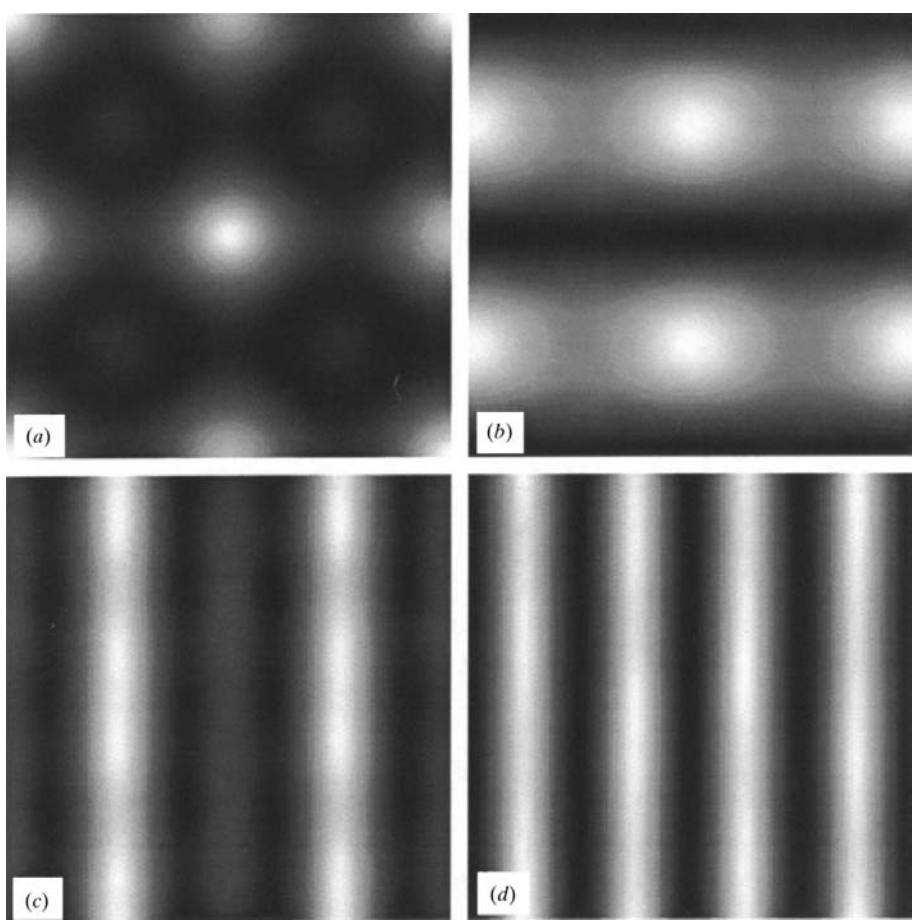

Fig. 6. Density maps of (*a*) first tightly bound 1*s*, (*b*) second free $2p_y$-like, (*c*) third free $2p_x$-like and (*d*) fourth free Bloch state with higher energy. All maps correspond to exact zone-axis incidence, *i.e.* $\mathbf{K}_t = 0$.

extinction distances in these regions are shortest, and that electrons in the transmitted beam will be firstly diffracted out of the transmitted beam into the diffracted beam resulting in dark contrast in the zero disc of the CBED pattern. Fig. 9(*g*) is a simulated zero disc of the CBED patterns for a crystal thickness of 250 Å, showing that this is indeed the case, *i.e.* as the crystal thickness increases from zero thickness, at which the corresponding zero CBED disc has no contrast, the outer regions towards the four edges of the pattern first meet their extinction distances and therefore result in dark contrast in the CBED pattern. As the crystal thickness increases further to 500 Å, *i.e.* approximately twice the extinction distance for the outer regions toward the four edges of the CBED disc, the electrons being diffracted out of the transmitted beam are diffracted back into the transmitted beam and the four edges appear bright again while the inner regions with longer extinction distances of about 500 Å begin to appear dark (see Fig. 9*h*). For a thicker crystal with a thickness of 2000 Å, Fig. 9(*i*) shows that more fringes appear in the disc and the central point appears dark. This is in contrast with the case of NiO where the contrast in the central region does not change much with changing crystal thickness. The reason for this is that, unlike in the case of NiO, where only one free Bloch wave is strongly excited near the zone-axis region, both Bloch waves numbers 1 and 2 have appropriate excitation amplitudes $\alpha^{(1)}$ and $\alpha^{(2)}$ for the exact zone-axis incidence resulting in strong thickness-dependent contrast *via* the interference between Bloch waves numbers 1 and 2. For the exact zone-axis incidence, the length of absorption ℓ for Bloch waves numbers 1 and 2 are 11 132 and 22 649 Å, respectively, and both lengths are much longer than the typical thickness used in electron-microscopy experiments, and this explains why the bound Bloch wave number 1 contributes in MgO but not in NiO.

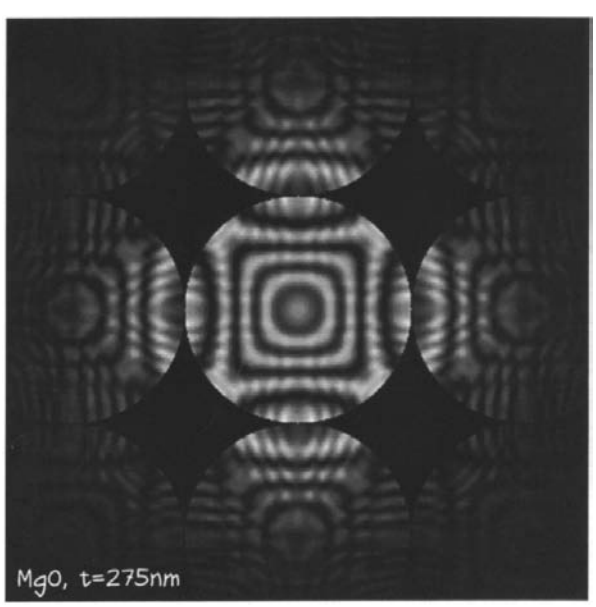

Fig. 7. Simulated $\langle 1\bar{1}1\rangle$ zone-axis CBED pattern for MgO, a primary-beam energy of 119.15 keV and a thickness of 2750 Å.

4. Conclusions

An off-axis ring pattern is observed in the $\langle 1\bar{1}1\rangle$ zone-axis CBED patterns from an NiO single crystal. We show that the off-axis ring pattern results mainly from interference between two most strongly excited free Bloch waves with anisotropic dispersive band structure, while the strongly excited tightly bound 1*s* Bloch state is attenuated rapidly and does not contribute significantly to the observed CBED contrast. For a material with the same sodium chloride structure but less scattering power, such as MgO, the bound 1*s* Bloch state is less

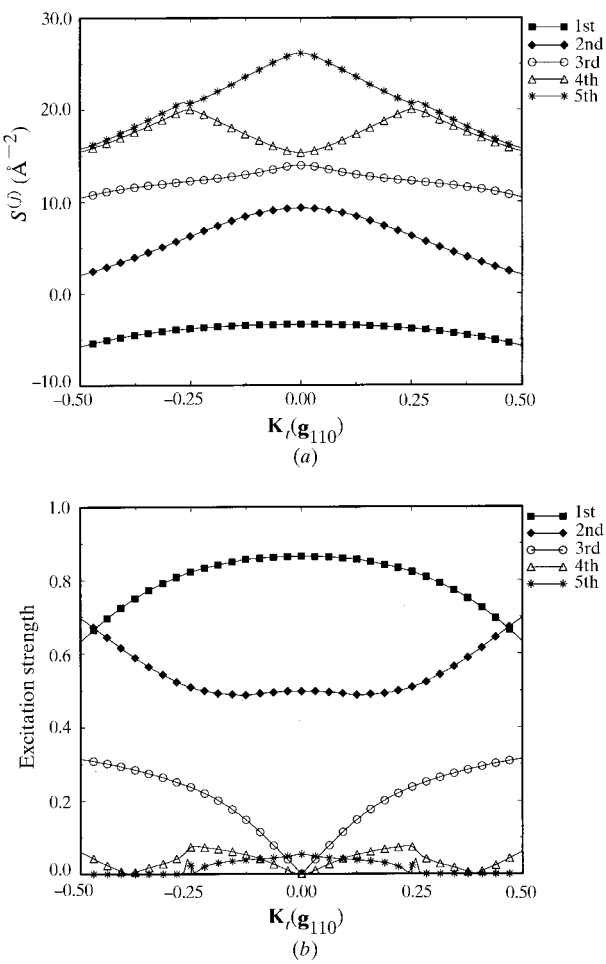

Fig. 8. Plots of (*a*) band structure $S^{(j)}(\mathbf{K}_t)$ and (*b*) Bloch-wave excitation strength $|\alpha^{(j)}(\mathbf{K}_t)|$ for the first five most strongly excited Bloch waves and an MgO single crystal.

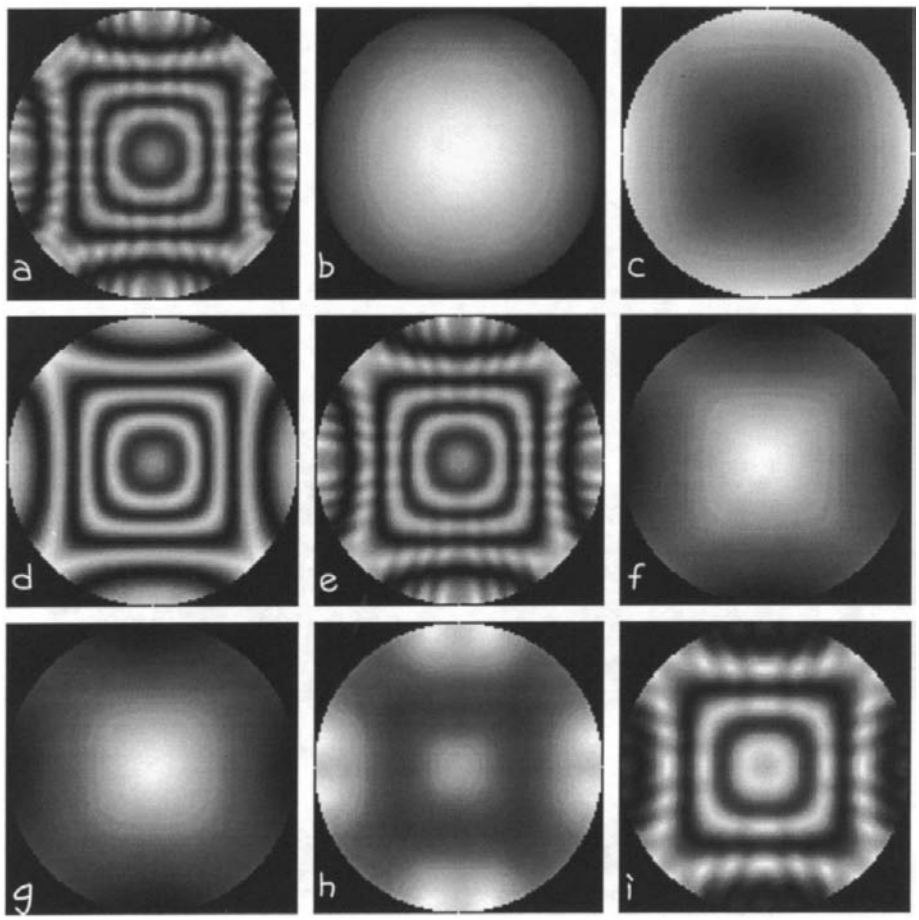

Fig. 9. Simulated CBED patterns for a series of crystal thicknesses (*a*) $t = 2750$ Å, (*g*) $t = 250$ Å, (*h*) $t = 500$ Å, (*i*) $t = 2000$ Å. Shown in (*b*) is the map of $S^{(1)}(\mathbf{K}_t)$ for the tightly bound 1*s* Bloch state and in (*c*) is the difference map of $S^{(2)}(\mathbf{K}_t) - S^{(1)}(\mathbf{K}_t)$. (*d*) is the CBED pattern formed by two Bloch waves, *i.e.* Bloch waves numbers 1 and 2, (*e*) is the same pattern formed by Bloch waves numbers 1, 2 and 3. (*f*) is the map of the extinction distance $\zeta^{(2-1)}(\mathbf{K}_t)$ between the Bloch waves numbers 1 and 2.

strongly absorbed and together with a strongly excited free Bloch state results in a more conventional zone-axis ring pattern similar to that observed in the ⟨001⟩ zone-axis CBED pattern of silicon (Tanaka & Terauchi, 1985).

This work was supported by the National Science Foundation of China and the NSF (grant No. 19425006). The authors thank Dr S. L. Dudarev for useful discussions on NiO and general diffraction phenomena.

References

Bethe, H. (1928). *Ann. Phys. (Leipzig)*, **87**, 55–129.
Bird, D. M. (1989). *J. Electron Microsc. Tech.* **13**, 77–97.
Eaglesham, D. J., Kvam, E. & Humphreys, C. (1988). *Inst. Phys. Conf. Ser.* **93**, 33–34.
Fung, K. & Steeds, J. (1984). *Philos. Mag.* A**50**, 25–44.
Gao, H., Peng, L.-M. & Zuo, J. (1999). *Acta Cryst.* A**55**, 1014–1025
Gjønnes, J., Olsen, A. & Matsuhata, H. (1989). *J. Electron Microsc. Tech.* **13**, 98–110.
Gjønnes, K., Gjønnes, J., Zuo, J. & Spence, J. C. H. (1988). *Acta Cryst.* A**44**, 810–820.
Hirsch, P. B., Howie, A., Nicholson, R., Pashley, D. & Whelan, M. (1977). *Electron Microscopy of Thin Crystals.* Malabar/Florida: Krieger Publishing Company.
Shannon, M. & Steeds, J. (1977). *Philos. Mag.* A**36**, 279–307.
Slack, G. (1960). *J. Appl. Phys.* **31**, 1571–1582.
Tanaka, M. & Terauchi, M. (1985). *Convergent-Beam Electron Diffraction.* Tokyo: JEOL Ltd.